Biochimica et Biophysica Acta 1837 (2014) 385–395

Contents lists available at ScienceDirect

Biochimica et Biophysica Acta

journal homepage: www.elsevier.com/locate/bbabio

Structural studies show energy transfer within stabilized phycobilisomes independent of the mode of rod–core assembly

Liron David [a], Mindy Prado [b,c], Ana A. Arteni [d], Dominika A. Elmlund [e], Robert E. Blankenship [b,c], Noam Adir [a,*]

[a] Schulich Faculty of Chemistry, Technion-Israel Institute of Technology, Haifa 32000, Israel
[b] Department of Biology, Washington University in St. Louis, St. Louis, MO 63130, USA
[c] Department of Chemistry, Washington University in St. Louis, St. Louis, MO 63130, USA
[d] IMPMC-UMR7590, CNRS-Université Pierre & Marie Curie-IRD, Paris 75005, France
[e] Stanford University Medical School, Dept. of Structural Biology, Stanford, CA 94305-5126, USA

ARTICLE INFO

Article history:
Received 19 October 2013
Received in revised form 19 December 2013
Accepted 30 December 2013
Available online 6 January 2014

Keywords:
Photosynthesis
Cyanobacteria
X-ray crystallography
Cryo transmission electron microscopy
Complex assembly

ABSTRACT

The major light harvesting complex in cyanobacteria and red algae is the phycobilisome (PBS), comprised of hundreds of seemingly similar chromophores, which are protein bound and assembled in a fashion that enables highly efficient uni-directional energy transfer to reaction centers. The PBS is comprised of a core containing 2–5 cylinders surrounded by 6–8 rods, and a number of models have been proposed describing the PBS structure. One of the most critical steps in the functionality of the PBS is energy transfer from the rod substructures to the core substructure. In this study we compare the structural and functional characteristics of high-phosphate stabilized PBS (the standard fashion of stabilization of isolated complexes) with cross-linked PBS in low ionic strength buffer from two cyanobacterial species, *Thermosynechococcus vulcanus* and *Acaryochloris marina*. We show that chemical cross-linking preserves efficient energy transfer from the phycocyanin containing rods to the allophycocyanin containing cores with fluorescent emission from the terminal emitters. However, this energy transfer is shown to exist in PBS complexes of different structures as characterized by determination of a 2.4 Å structure by X-ray crystallography, single crystal confocal microscopy, mass spectrometry and transmission electron microscopy of negatively stained and cryogenically preserved complexes. We conclude that the PBS has intrinsic structural properties that enable efficient energy transfer from rod substructures to the core substructures without requiring a single unique structure. We discuss the significance of our observations on the functionality of the PBS *in vivo*.

1. Introduction

In photosynthesis, the capture and transfer of light energy to photosynthetic reaction centers serves as the initial step in solar energy storage and is performed primarily by light harvesting complexes (LHCs) [1,2]. LHCs from almost all photosynthetic organisms, either oxygenic or anoxygenic, share many of the same functional characteristics while differing greatly in the molecular details of how this critical functionality is achieved. LHCs are composed of proteins that bind pigments (chlorophylls, bilins or carotenoids) in specific positions, orientations and conformations enabling the efficient absorption and transfer of energy. Absorbed energy is typically funneled down an energy gradient into photochemical reaction centers (RC) where charge separation is achieved. The LHC protein must also have the ability to self-assemble into complexes [3,4], which may require enzymatic or chaperone activities. In many cases, assembly is a multi-level process, with the initial assembly of subcomplexes (consisting of the basic monomeric peptides and appropriately bound chromophores), followed by the assembly into a complete complex, and then followed by further assembly into supramolecular systems that contain an entire energy funnel coupled to an RC. The requirement of multiple components indicates that the overall mechanism of energy transfer may benefit from the existence of short-range localized energy transfer processes (within each sub-complex), which are coupled together to enable transfer over larger distances [5]. One role of correctly assembling a multi-complex system is to bring pigments of one sub-complex into close and optimal proximity to that of an adjacent complex, thus facilitating directional energy transfer kinetics. Specific mechanisms must also exist to enable the dis-connection of LHCs or their complete disassembly [6], according to the environmental conditions of the organism. Since efficient energy transfer requires precision in the positioning of the various components, it is typically assumed that each LHC has a unique structure (*i.e.* a structure that orients all chromophores in an optimal fashion for

Abbreviations: Am-clPBS, *A. marina* cross-link stabilized phycobilisome; Am-hpPBS, *A. marina* high phosphate stabilized phycobilisome; APC, allophycocyanin; HPB, high concentration phosphate buffer; LHC, light harvesting complex; LP, linker protein; PBP, phycobiliprotein; PBS, phycobilisome; PC, phycocyanin; PCB, phycocyanobilin; PE, phycoerythrin; PEC, phycoerythrocyanin; PSII, Photosystem II; RC, reaction center; Tv-clPBS, *T. vulcanus* cross-link stabilized phycobilisome; Tv-hpPBS, *T. vulcanus* high phosphate stabilized phycobilisome

* Corresponding author. Tel.: +1 972 4 8292141; fax: +1 972 4 8295703.
E-mail address: nadir@tx.technion.ac.il (N. Adir).

0005-2728/$ – see front matter © 2014 Elsevier B.V. All rights reserved.
http://dx.doi.org/10.1016/j.bbabio.2013.12.014

energy transfer that outcompetes by orders of magnitude all other modes of de-excitation) and mode of assembly.

The phycobilisome (PBS) is the major LHC in cyanobacteria and red algae and is considered as one of the most efficient LHCs with ~95% efficiency in energy transfer to the terminal emitter [7,8]. The PBS is distinguished from other LHCs both in size and pigment content, being 1–2 orders of magnitude larger than the LHCs found in plants, algae and purple bacteria, with a molecular weight between 3 and 7 MDa and dimensions (as determined by negatively stained transmission electron microscopy (TEM) images) of at least 12 × 40 × 60 nm [9,10]. The PBS is attached to the stromal surface of the thylakoid membrane and is assembled from pigmented proteins referred to as phycobiliproteins (PBPs) and unpigmented proteins called linker proteins (LPs), sequestered in large apertures formed by the association of the PBPs into circular assemblies. There are four major forms of PBPs which absorb between 550 and 680 nm (an absorption range that covers much of the segment of the sun's energy not covered by the chlorophyll *a* or chlorophyll *a*/*b* based LHCs), classified by the type and number of linear tetrapyrrole pigments (bilins) that they covalently bind. These are phycoerythrin (PE, $\lambda_{max} = 560$ nm), phycoerythrocyanin (PEC, $\lambda_{max} = 575$ nm), phycocyanin (PC, $\lambda_{max} = 620$ nm) and allophycocyanin (APC, $\lambda_{max} = 652$ nm). Organisms containing the PBS are thus able to utilize a much larger fraction of the visible spectrum for photosynthesis. The building blocks of all PBPs in the complex are two homologous subunits, α and β, forming the (αβ) monomer. Three (αβ) monomers then associate to form a trimer, shaped as a hollow disk. In PC, PE and PEC, two trimers associate to create a hexamer, shaped as a double disk and hexamers associate further to form rod shaped aggregates, with a total of 6–8 rods per PBS. APC trimers form cylinders containing two to four trimers and two to five of these cylinders pack into the core sub-complex. The structural information on the LPs is very limited. A LP, together with a PBP, has been seen only in the structure of trimeric APC with the L_c core linker [11] (PDB ID: 1B33). Recently, structures of several short domains from L_R linker (the main rod linker) and L_{CM} (core membrane linker) were determined by NMR or X-ray crystallography (PDB IDs: 2KY4, 2L06, 2L8V, 3OHW, 3OSJ, 3RPU, 2NPH).

Isolated PBPs were among the first structures of photosynthetic proteins to be determined [9]. However while other LHC structures have now been determined in their entirety [12–15], the complete structure of the PBS has been elusive. The difficulty in determining such a structure is not only due to its massive size, but also due to its extreme lack of stability *in vitro* coupled with native and isolation-induced heterogeneities [16]. From a structural point of view, the architecture of the entire PBS has been visualized at low resolution by TEM of negatively stained isolated particles [17–23], showing the rod and core assemblies. The EM micrographs published over the years of isolated PBSs from a large variety of cyanobacteria and red algae exhibited a high degree of heterogeneity in the number of rods and core cylinders and in the positions of the rods surrounding the central core [20]. Even in high concentrations of phosphate buffer (>0.7 M; HPB), the most efficient PBS stabilizing agent, different stages of complex disassembly can be identified in most micrographs, with many of the rods disconnected and found at odd angles from the core. Some TEM-based models suggested that the rods are positioned around the core in one of a number of radial arrangements [8,24], either all in the same plane (of the core cylinders) or in some sort of staggered arrangement. A second model proposed that the rods are arranged in pairs, in a way that two rod doublets are parallel to the thylakoid membrane and one rod doublet is perpendicular to the membrane [7,9]. This model is consistent with some of the crystal structures of rod PBP components. This arrangement could provide more inter-rod contacts (perhaps facilitating inter-rod energy transfer) and does not require a staggered assembly of the rods onto the core cylinders due to a mismatch of the circumference of the core and the rod diameters.

In this report we present spectroscopic analysis of PBS that remain functional in the absence of high concentrations of phosphate buffer due to stabilization by chemical cross-linking. Two very different PBSs, from *Thermosynechococcus vulcanus* (TvPBS) and *Acaryochloris marina* (AmPBS) were analyzed by spectroscopic and single crystal confocal microscopy. The cross-linked TvPBS was also analyzed by cryo-TEM, and X-ray crystallography of single crystals, indicating that energy transfer from rods to cores does not require a specific, unique assembly. The possible functional aspects of these observations are discussed.

2. Methods and materials

2.1. PBS purification

T. vulcanus were grown in a 10 liter cylinder at 55 °C in the presence of 5% CO_2 with continuous illumination at ~35 μE. Cells were harvested after 5–7 days of growth by centrifugation at 5000 rpm (Sorvall T21 centrifuge; 3000 ×*g*) for 10 min. The resulting pellet of cells was frozen at −20 °C. 5–10 g of frozen cells were resuspended in 0.9 M phosphate buffer pH 7.0 and disrupted by one treatment in a French pressure cell at 20,000 psi. The lysate was then centrifuged at 15,000 rpm (27,000 ×*g*) for 30 min at 4 °C. The pellet was resuspended with 0.9 M phosphate buffer and incubated for 1 h with 2% Triton X-100 (w/v, Sigma), followed by clarification by centrifugation. The resulting supernatant was centrifuged (Beckman Coulter, optima L-90K ultracentrifuge, Beckman Type T70.1 rotor) in 10 ml tubes for 2.5 h at 40,000 rpm (147,000 ×*g*) and the resulting blue pellet was resuspended with 0.9 M phosphate buffer and placed on a 0.8 M sucrose cushion and centrifuged for 2.5 h at 40,000 rpm (147,000 ×*g*). The resulting pellet was resuspended with 0.9 M phosphate buffer and placed on a three-step sucrose gradient constructed by 1 M, 1.25 M and 1.5 M sucrose in the presence of 0.9 M phosphate. The sucrose gradient was centrifuged overnight at 45,000 rpm (186,000 ×*g*) and three to four different fractions were isolated from the sucrose gradient. These are denoted Tv-hpPBS throughout the manuscript.

A. marina cells were grown in a 25 liter bioreactor. The preparation was made from 30 to 40 g of cells that were resupended in HPB. The cells were broken using sharp silicon carbide beads and a bead beader (Bio-Spec Products) or vortex for 5 times, 30 s for each time (with 5 min incubation). After cell breakage, centrifugation and Triton treatment (as performed for *T. vulcanus* PBS), the supernatant was centrifuged at 55,000 rpm (278,000 ×*g*) overnight resulting in a blue pellet. A highly concentrated and homogenous fraction of PBS was isolated at 0.75 M sucrose from 0.3 to 0.75 M sucrose gradient in the presence of 0.9 M phosphate centrifuged at 55,000 rpm (278,000 ×*g*) overnight. This fraction was further purified by an additional 0.3–0.75 M sucrose gradient.

2.2. Cross-linking of Tv-hpPBS and Am-hpPBS

Pellets of Tv-hpPBS or Am-hpPBS obtained from the first 0.8 M sucrose cushion mentioned in the previous section was resuspended with 0.9 M phosphate buffer and placed on a step gradient with the following composition: 0.9 M sucrose, 1 M sucrose with 0.05% (w/v) Glutaraldehyde (GA, Sigma), 1.1 M sucrose with 0.15% GA and 1.25 M sucrose with 0.25% GA. All steps include the presence of 0.9 M phosphate. The cross-linking gradient was centrifuged for a short time at a high speed (45 min at 55,000 rpm; 278,000 ×*g*) in order to prevent the PBS from being cross-linked to a higher degree. The resulting pellet was solubilized in 50 mM Tris pH 8.0 (Buffer A) and loaded onto a three step sucrose gradient of 1.25 M, 1.5 M and 1.75 M in buffer A. After centrifugation for 3 h at 50,000 rpm (229,000 ×*g*), a pellet was obtained which was resupended in buffer A. Finally, this suspension was placed on another step gradient of 1.75 M, 2 M and 2.25 M sucrose in buffer A, and a single band of PBS was obtained at the interface between 2 and 2.25 M sucrose (further denoted Tv-clPBS). Cross-linked PC or APC, did not penetrate this final gradient.

For Am-hpPBS crosslinking, Am-hpPBS was placed on a step gradient composed of 0.15 M sucrose with 0.05%GA, 0.3 M sucrose with 0.10%

GA and 0.5 M sucrose with 0.15% GA. The gradient was centrifuged for 3 h at a high 55,000 rpm (278,000 ×g). This ultracentrifugation process resulted in two fractions at 0.3 M and 0.5 M sucrose. The fraction isolated at 0.5 M sucrose was loaded on an addition step gradient of 1.25 M, 1.5 M and 1.75 M sucrose in 50 mM Tris. After ultracentrifugation for 3 h at 50,000 rpm Am-clPBS was obtained at the interface between 1.5 and 1.75 M sucrose.

2.3. PBS crystallization

All crystallization experiments were performed using the hanging drop vapor-diffusion method in a 24-well tissue-culture plate at 20 °C. Crystallization drops were formed by mixing 2 μl (10–15 mg/ml) protein with 2 μl precipitant above 0.6 ml reservoir well solution. Tv-hpPBS crystals were obtained by adding 10–20 mg/ml BSA to the crystallization drop with a ratio of 1:1 between hpPBS and BSA. The crystallization drop was placed above 1.2–1.4 M phosphate buffer pH 7.0 with 0.8 M sucrose reservoir. Tv-clPBS crystals were obtained within 3–4 days in 3 different crystallization conditions: i) 1.4 M phosphate buffer; ii) 1 M sucrose pH 7.0; 35% Tascimate pH 7.0 and iii) 1 M $AmSO_4$, 1% PEG 3350, 0.1 M Bis–Tris pH 5.5.

2.4. Isolated complex and crystal analysis

All isolated samples were characterized by SDS-PAGE, absorption (Varian spectrophotometer — Cary Bio 50) and fluorescence spectroscopy at 77 K (Flourolog, excitation at 580 nm, with slit width of 5 nm for excitation and 1 nm for emission). Fluorescence emission spectra of single crystals were measured by using a LSM 510 META laser scanning confocal microscope (Zeiss) with a DPSS laser with excitation line at 561 nm. The focus was reduced to a spatial resolution of 1 μm^3, and the crystals were typically 10–30 μm in depth [16].

For further analysis, crystals were extensively washed in the crystallization mother liquor and then solubilized in water. The resulting proteins were characterized by SDS-PAGE, mass spectrometry (Tandem RPLC-ESI-MS, Smoler Proteomics Centre, Technion — Israel Institute of Technology) [16], or absorption/fluorescence spectroscopy.

2.5. Data collection and X-ray structure determination

X-ray diffraction data from hpPBS and clPBS crystal was collected at the European Synchrotron Radiation Facility (ESRF) on beamlines ID23-2 and ID23-1, respectively.

hpPBS diffracted to 3.5 Å and the final model was refined to 3.7 Å, whereas clPBS crystals diffracted to a higher resolution of 2.2 Å and the final model was refined to 2.4 Å. The data sets for both Tv-hpPBS and Tv-clPBS were scaled and merged using MOSFLM [25] and molecular replacement was carried out with Phaser [26] using the 3O18 structure as a search model. The structure of clPBS was refined using CNS [27] and manual modifications were made using Coot [28]. All structural visualization and analysis were performed using PyMOL [29]. Structural alignments (all atom and main chain) were carried out using Coot.

2.6. PBS negative stained EM

The grids for negative staining were prepared according to Arteni et al. [22], where a sample of isolated PBS is placed on the grid, fixed by using 0.5% GA, washed with ammonium acetate (10 mM, 50 mM and 100 mM) and finally stained by using 2% uranyl acetate. The samples were viewed at various EM facilities and the images were recorded on CCD cameras. Negatively stained TEM measurements for fresh hpPBS were performed and were measured at CEA, Saclay, France using a Philips CM120 electron microscope. Tv-clPBS and Am-clPBS were imaged using a Technai G2 spirit BioTWIN and JEOL 1200EX electron microscopes operating at 80 kV.

2.7. PBS cryoEM

Tv-clPBS was observed by using cryo TEM at the Department of Structural Biology of Stanford University. Briefly, clPBS was applied to glow discharged grids for 60 s, and then blotted for 3.5 s before plunging into liquid ethane. The grids were examined with a CCD camera (4 K × 4 K Gatan Ultrascan™ 4000) under low-dose conditions (each exposure approximately $15e^{-}Å^{-2}$) on a Tecnai F20 microscope (FEI) operating at 200 kV. The CTF parameters were determined using CTFFIND3 (ref — http://www.ncbi.nlm.nih.gov/pubmed/?term=grigorieff+ctf) and phase-flipped in Spider [30]. Individual particles were picked in Boxer a part of EMAN package [31], and processed in SIMPLE [32].

2.8. Accession numbers

Coordinates and structure factors have been deposited in the Protein Data Bank with the following accession entry: Crystals of cross-linked stabilized and functional phycobilisomes: only phycocyanin rods contribute to diffraction (PDB ID: 4N6S).

3. Results

3.1. Characterization of the T. vulcanus PBS stabilized in phosphate buffer or by chemical cross-linking

PBSs from *T. vulcanus* in the presence of 0.9 M phosphate (Tv-hpPBS) were isolated (see Methods and materials section) by sucrose gradient ultracentrifugation. In most cases, the gradients separated between three and four distinct bands that showed the presence of intact and functional PBS as determined by energy transfer from PC to APC. These different fractions exhibited minor differences in their fluorescence and absorbance spectra and in their protein content as analyzed by SDS-PAGE. It cannot reliably be determined whether the observed heterogeneity in the isolated PBS is due to heterogeneities in the natural population of the PBS *in vivo*, or whether the process of isolation induces such heterogeneities. It is quite likely that there is a combination of both of the above reasons as causes of heterogeneity in the isolated complex.

In order to be able to obtain more homogeneous PBSs and to stabilize the complex so that it could be analyzed in low ionic strength buffers, we performed mild cross-linking with GA. Our procedure for gradual cross-linking of the PBS was developed by modifying the GraFix method for preparing cryoEM samples [33]. By this method we formed mostly intra-molecular contacts and prevented the formation of inter-molecular contacts between complexes. Immediately following cross-linking, the PBSs are transferred to a 50 mM Tris buffer, pH 8.0 (buffer A), thus allowing all non-cross-linked PBSs to disassemble. The PBS typically disassembles into trimeric rings and all interactions between the LPs and the rings are lost. The cross-linked PBS (Tv-clPBS) was further purified by sucrose gradients and a single band was isolated at the interface between 2 and 2.25 M sucrose in buffer A [34].

Isolated Tv-clPBS was spectroscopically compared to the intact fraction of Tv-hpPBS. Both Tv-clPBS and Tv-hpPBS fractions exhibited similar spectroscopic properties in their room temperature (RT) absorbance and both RT and 77 K fluorescence spectra (Figs. 1A, B and 2A). The absorbance spectra of Tv-hpPBS show a maximum at 635 nm with a shoulder at 652 nm, as expected for an intact PBS. Tv-clPBS also showed a maximum at 635 nm with a slightly more significant shoulder at 652 nm in comparison to Tv-hpPBS. This indicates that while both fractions contain intact PBS, the Tv-clPBS fraction may have some shorter rods, and thus exhibits a slightly higher APC/PC ratio (Fig. 1A). In addition, both Tv-hpPBS and Tv-clPBS showed the same fluorescence emission maximum at RT with a significant shoulder at 680 nm when the samples were excited at 580 nm (Fig. 1B). Dynamic light scattering measurements indicated that over 90% of the Tv-hpPBS had a

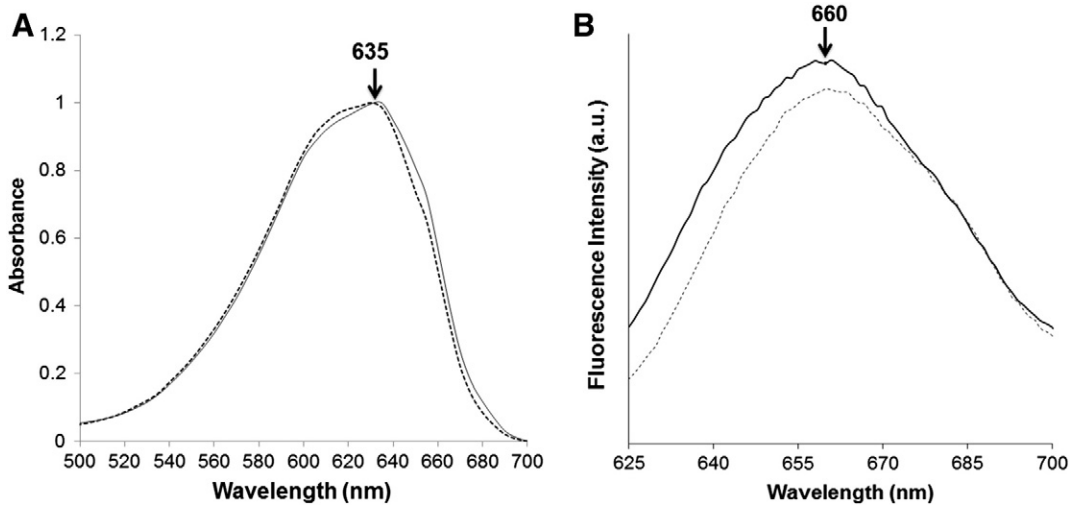

Fig. 1. Cross-linking preserves TvPBS energy transfer at low ionic strength. (A) Room temperature absorption and (B) Fluorescence emission spectra (λ_{ex} = 580 nm) of Tv-hpPBS (0.9M phosphate, dashed lines) or TV-clPBS (solid lines).

hydrodynamic radius of 17 nm, indicating a molecular mass of about 3 MDa (data not shown).

In order to determine whether the Tv-clPBS was not only intact but also functional in efficient energy transfer between PC and APC, its low-temperature fluorescence emission spectrum was measured and compared to that of Tv-hpPBS (Fig. 2A). The 77 K emission spectra were obtained at equivalent absorption at 635 nm and were incubated in the appropriate buffer (Buffer A or HPB) at RT for 1 h prior to freezing. The fluorescence spectra show that prior to, and following cross-linking, the emission maxima were at 680 nm with a shoulder at 660 nm and the fluorescence intensity at the emission maxima at 680 nm was similar (Fig. 2A). The emission intensity of Tv-clPBS sample was actually slightly higher than the Tv-hpPBS before cross-linking. This indicates that our method has indeed cross-linked the PBS in a very gentle fashion that does not interrupt the PBS energy transfer function. When the Tv-hpPBS was diluted into buffer A, the complex quickly disassembled and there was a significant blue shift in the fluorescence maximum to 645 nm, which correlates to an emission from PC trimers, and a smaller component from APC trimers at 660 nm. Thus, not only are the rods in the Tv-clPBS competent in energy transfer to the core, but the core is functional in energy transfer from APC to the terminal emitters α^B and ApcE.

3.2. Stabilization of isolated A. marina PBS by cross-linking

In order to broaden the scope of stabilizing functional PBS in low ionic strength buffers, we applied the same protocol to the PBS isolated from other species. Results similar to those obtained for *T. vulcanus* were also obtained for *Synechocystis* PCC sp. 6803 PBS (data not shown) and *A. marina* PBS (AmPBS). *A. marina* is a unique cyanobacterium whose major pigment is chl *d* instead of chl *a* [35–37]. *A. marina* has the simplest and smallest PBS from all the known PBSs. Its molecular weight is only about 1 MDa, and based on EM micrographs [38,39] and biophysical experiments is assembled as a single rod, containing three PC hexamers and a single, terminal mixed hexamer of one PC trimer and one APC trimer. Whole cell TEM of *A. marina* cells appears to show PBSs aligned one next to the other in a semi-crystalline array [37]. Energy transfer between PC and APC is quite efficient, although this mode of relative orientation is diametrically different than that suggested for all other PBSs. We isolated AmPBS in HPB (Am-hpPBS)

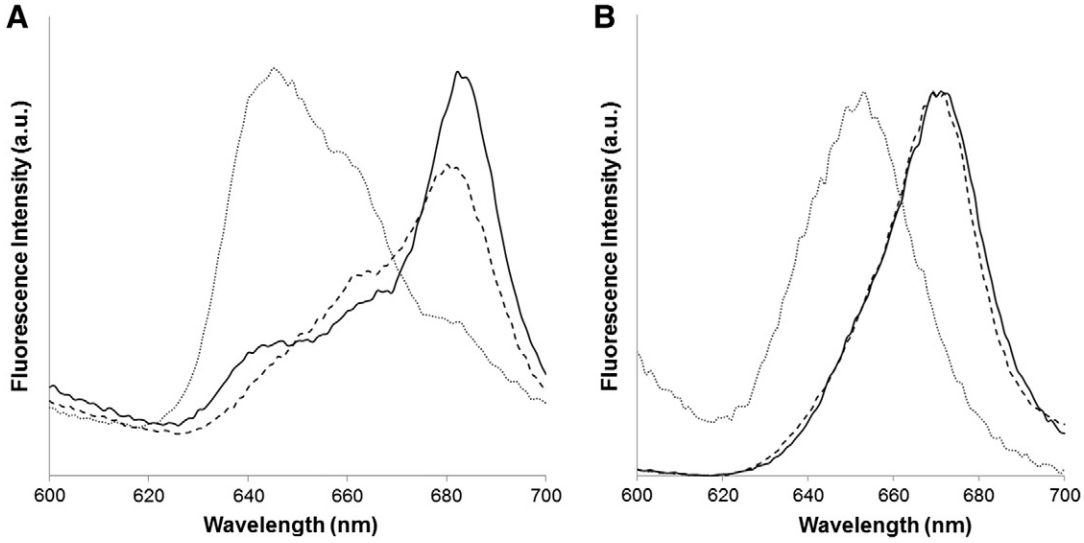

Fig. 2. Low temperature TvPBS and AmPBS fluorescence emission spectra before and after crosslinking. (A) 77 K fluorescence emission spectra (λ_{ex} = 580 nm) were obtained for hpPBS (dashed line), hpPBS diluted into 50 mM Tris pH = 8.0, 1 hour prior to freezing (dotted line) or clPBS in 50 mM tris pH = 8 (solid line). (B) 77 K fluorescence (λ_{ex} = 580 nm) of Am-hpPBS in 0.9 M phosphate (dashed line), Am-clPBS following cross-linking in 50 mM Tris pH = 8.0 (solid line) or Am-hpPBS following transfer to 50 mM Tris pH = 8.0 (dotted line).

and performed size analysis by fluorescence correlation spectroscopy [40] (FCS, Table S1). FCS showed that the Am-hpPBS were intact and of the correct size. The analysis showed a correlation that was best fit by two components, a very fast component that had a diffusion time of ~100–120 μs (equivalent to a particle of the dimensions of stable trimers) and a slow component that had a diffusion time of ~1400 μs (equivalent to intact AmPBS). Analysis of the Photon Count Histogram (PCH)[40] that was performed for the well fitted samples allowed us to determine the difference in brightness between the trimers and the entire PBS. The entire AmPBS contains 69 cofactors whereas the PC trimer contains 9 cofactors, therefore the ratio of brightness between them should be 7.7, very near the measured difference in brightness for the AmPBS solution, which was found to be 7.0. The calculated molecular weight of the isolated Am-hpPBS was 1.4 MDa, which is consistent with the theoretical molecular weight of 1.2 MDa.

The AmPBS also requires HPB to prevent disassembly, so we performed the same gradual cross-linking protocol to Am-hpPBS. The cross-linked AmPBS (Am-clPBS) was further purified by isolating two fractions from the interface between 1.5 and 1.75 M sucrose in buffer A. The Am-hpPBS and Am-clPBS gave the same absorbance maxima at 618 nm and 77 K fluorescence emission from both samples showed the same maximum at 670 nm (Fig. 2B). This indicates that as for the TvPBS, our method indeed enables the isolation of active and intact complexes in low salt buffers, with efficient energy transfer from PC to APC.

Mass spectrometric peptide identification by tandem RPLC-ESI-MS (MS, Table S2) of Am-hpPBS and Am-clPBS showed the presence of four gene products from multiple genes encoding for the α and β subunits of PC, and two LPs. This analysis also identified which subunits cross-linked to other subunits (Table S3), and showed that the heterogeneity is within the PBS, not in different PBS particles. It could not be determined whether the heterogeneity is on the level of the entire rod, with hexamers or even within single trimers since the length of GA could afford crosslinks across the molecular interfaces of each of these levels of assembly. These results indicate that isolated AmPBS is more heterogeneous than other PBSs, such as those of *T. vulcanus*. Peptides from APC could not be identified in the MS analysis; however since the isolated AmPBS maximal fluorescence is clearly at 670 nm, this indicates that APC is present. The anomalous behavior of APC in the MS analysis requires further study.

3.3. Crystallization of TvPBS and AmPBS

The primary method for high-resolution structural analysis of large complexes is by X-ray crystallography. We attempted to crystallize the entire PBS, maintaining complex integrity by the presence of HPB in all the crystallization screens. Crystallization trials of Tv-hpPBS were performed with a variety of commercial crystallization screens; however, either no crystals were obtained or small crystals containing trimeric PC crystals (based on spectroscopic and SDS-PAGE analysis) appeared. This indicates that the PBS disintegrates slowly (over weeks) even in the presence of HPB. In order to overcome disassembly, we conjectured that we could perhaps improve long-term complex stability by mimicking the very crowded environment in which the PBS is surrounded *in vivo* [41]. *In vitro* molecular crowding was performed by addition of 10–20 mg/ml of bovine serum albumin (BSA) to the crystallization drops. In the presence of BSA, small blue crystals, shaped as half-moons were obtained after two weeks. The dimensions of the largest crystals were 50–100 μm and ~10 μm thick. In order to verify that the crystals contained functional and intact PBS (and that they were not crystals of trimeric PC to which uncrystallized PBS might adsorb), we collected and extensively washed crystals in 0.9 M phosphate buffer and then analyzed solubilized crystals by MS and single crystal confocal fluorescence emission microscopy. MS analysis of Tv-hpPBS crystals (Table 1) shows that all of the components associated with the PBS complex were indeed present, including all of the PBPs (including minor APC variants, α^B and β^{18}) and all LPs, including ApcE (also referred to as L_{CM}), the core–membrane linker that facilitates PBS assembly and attachment to the thylakoid membrane. MS identified peptides corresponding to the presence of full length 127 kDa ApcE linker, as predicted from the sequence of the *T. elongatus apcE* gene. Such a large ApcE protein indicates that the TvAPC is most likely a pentacylindrical PBS. Although present at high concentration in the crystallization liquor, only a very small coverage (<9%) was obtained for peptides derived from the BSA used during crystallization, indicating that the procedure of washing the crystals was efficient and that the MS analysis was relevant for the actual contents of the PBS crystals.

RT fluorescence of single Tv-hpPBS crystals was measured by using confocal microscopy in a fashion previously used for rod crystals [16]. Confocal microscopy afforded measurement of the fluorescence at different positions and depths (to a resolution of 1 μm^3) and conclusively showed that the crystals were functionally homogenous. The results (Fig. 3A) show that the emission spectrum of a single crystal from the center of the crystal, when excited at 561 nm, results in a broad emission peak at 658–659 nm. These results actually show improved energy transfer between the rods and the core APC components as compared to the RT emission of the Tv-hpPBS in solution prior to crystallization (Fig. 1B), indicating that Tv-hpPBS crystals contain intact and functional PBSs and that the crystal lattice stabilizes the rod–core interaction, supporting improved energy transfer. The emission maxima from

Table 1
Mass spectrometric analysis of Tv-hpPBS and Tv-clPBS.

Subunit	% coverage[a] Tv-hpPBS crystals	% coverage[a] Tv-clPBS[b] solution	% coverage[a] Tv-clPBS[b] crystals	Gene	Function
αAPC	62	80.2	37.3	*apcA*	PBP[c]
βAPC	80	84.5	36.4	*apcB*	PBP
αPC	65	65.4	27.3	*cpcA*	PBP
βPC	89	93.0	42.4	*cpcB*	PBP
L_R^{30}	42	33.1	4.11	*cpcC*	Rod linker
$L_R^{7.8}$	49	69.2	N.D.	*cpcD*	Rod capping linker
L_{RC}^{30}	39	49.8	9.6	*cpcG4*	Rod–core linker
L_{RC}^{29}	24	34.3	4.1	*cpcG1*	Rod–core linker
L_{RC}^{31}	17	48.4	N.D.	*cpc*G2	Rod–core linker
L_C	27	37.3	N.D.	*apcC*	Core linker
α^B	27	35.1	N.D.	*apcD*	PBP[d]
L_{CM}	31	48.3	8.3	*apcE*	Core–membrane linker[e]
β^{18}	26	37.3	12.4	*apcF*	PBP[f]

[a] Percent of all potential peptides obtained by trypsin treatment prior to MS analysis.
[b] Only non GA cross-linked peptides.
[c] Phycobiliproteins.
[d] Two copies per PBS, terminal emitter, fluoresces at 680 nm.
[e] Two copies per PBS, terminal emitter fluoresces at 680 nm.
[f] Two copies per PBS, forms monomer with LCM subunit.

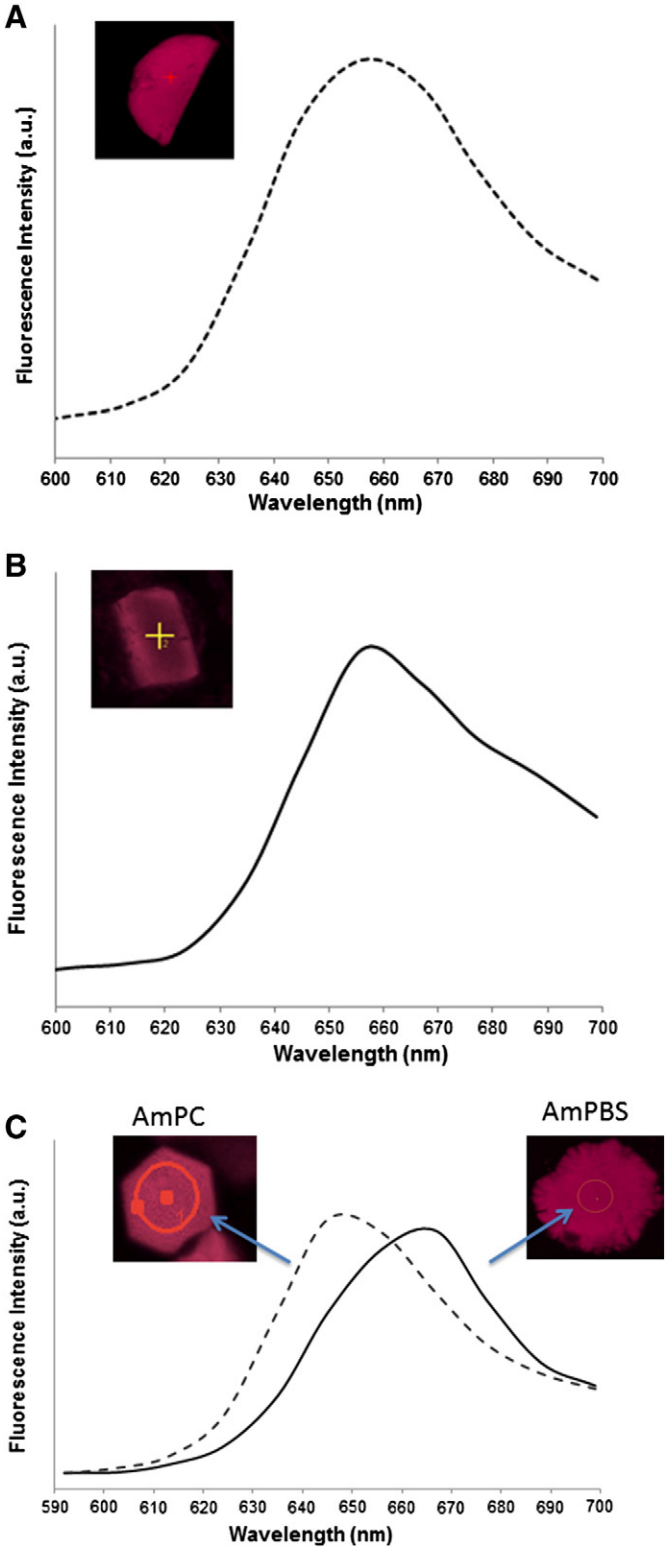

Fig. 3. Energy transfer from PC to APC occurs in Tv-hpPBS, Tv-clPBS and AmPBS single crystals. Fluorescence emission from Tv-hpPBS (panel A), Tv-clPBS (panel B), and Am-hpPBS (panel C, solid line) and Am-PC (panel C, dashed line) crystals by confocal fluorescence microscopy. Crystals were excited with a DPSS laser at 561 nm. Emission spectra shown were from the middle 1 μm^3 of each crystal (the resolution of the microscope). Insets show low-magnification images of the crystals in the confocal microscope, with the cross showing the position of fluorescent measurement.

similarly measured TvPC or TvRod crystals have been shown to be at 649 nm and 655 nm, respectively [16]. We have also obtained a few very small and dis-ordered crystals containing only the core-subcomplex (data not shown). These crystals showed a maximal fluorescence at 668 nm [42].

Tv-clPBS was set up for crystallization under the same conditions as for Tv-hpPBS in addition to screening for various alternative conditions. A small number of blue crystals of Tv-clPBS were obtained after a few days in the same conditions that afforded Tv-hpPBS crystals, however BSA was not required in the crystallization liquor. Additional crystals of Tv-clPBS were obtained in two other crystallization conditions and their morphology was different from the half-moon crystals (see Methods and materials for details). In addition to screening the crystals by X-ray diffraction, the Tv-clPBS crystals were also analyzed by confocal microscopy and MS in order to determine whether the new Tv-clPBS crystals contain intact and functional PBS. Confocal microscopy of a single Tv-clPBS crystal also shows a broad emission spectrum with a maximum at 659 nm with a more significant shoulder at 680 nm, compared to single Tv-hpPBS crystals (Fig. 3B). Thus the Tv-clPBS shows improved energy transfer to the terminal emitters, ApcE and α^B. MS results were obtained from a few crystals that were stable when washed and solubilized in Buffer A. The lower coverage of the identified peptides (in comparison to the coverage obtained from Tv-clPBS prior to crystallization) is a result of the significantly smaller number of crystals that were available for MS analysis, as well as the loss of all peptides that formed cross-links, since these have altered molecular weights (Table 1).

Am-hpPBS as well as Am-PC (obtained from disassociated PBS within the sucrose gradients), isolated in HPB as described above, were also crystallized in conditions similar to those for the Tv-hpPBS. In the Am-PC sample we obtained small hexagonal crystals, while in the AmPBS we obtained crystals lacking clear facets. Confocal fluorescence microscopy clearly showed that the hexagonal crystals contain only PC (Fig. 3C, dashed line), while the crystals grown from the isolated Am-hpPBS indeed contained the entire AmPBS (Fig. 3C, solid line) exhibiting efficient energy transfer from PC to APC. Diffraction was poor from all Am-hpPBS and Am-PC crystals perhaps due to the intrinsic heterogeneity in the AmPBS already described above.

3.4. Crystal structure of the T. vulcanus PBS

Tv-hpPBS crystals were screened on the microfocus beamline ID23-2, ESRF, with some crystals diffracting to 3.5–4 Å. We collected a full data set from a single Tv-hpPBS crystal to a resolution of 3.5 Å. We determined that the unit cell of the crystal was much smaller than was expected for an asymmetric unit that could contain a complete PBS according to models based on TEM. The data reduced to the H32 space group with unit cell dimensions that are similar to those of crystallized trimeric PC. The structure could be solved by molecular replacement with one PC monomer in the asymmetric unit. The structure was refined to 3.7 Å and the electron density maps indeed showed a monomer in the asymmetric unit. Disorganized electron density could be detected in the center of the trimeric disk where the linker proteins should be located.

According to the crystallographic data we concluded that Tv-hpPBS was arranged in the crystal as elongated rods and the extra electron density was a result of averaging all the different linkers in the complex. In addition, it would appear that while all of the APC components are present in the crystal, they do not significantly contribute to the crystal diffraction and thus are absent in electron density maps. This observation, coupled with the confocal microscope measurements indicate that PC and APC from *T. vulcanus* can associate in a co-linear fashion in long rods, without loss of efficient energy transfer. This arrangement of PC/APC association is reminiscent of that found in the PBS of *A. marina*.

Since it would seem that a major change in the PBS assembly appeared to occur during crystallization, we hoped that perhaps a different result would occur with the Tv-clPBS. Tv-clPBS crystals were screened at the ESRF on beamline ID23-1 and we were able to collect

a complete data set to 2.4 Å (Table S4). Analysis of the diffraction pattern determined that the space group and unit cell were similar to that obtained for the Tv-hpPBS crystals. The structure was solved by molecular replacement [26,43] and refined to 2.4 Å with CNS [27] (Table S4). It was thus apparent that Tv-hpPBS and Tv-clPBS are arranged in the crystal at the same manner. In both cases, the PC hexamers organize themselves into extended and organized rods that contribute to the crystal diffraction. All of the core components appear to be positioned randomly within the crystal, and thus do not contribute to the diffraction. Since these randomly placed components disrupt the crystal lattice, it is not surprising that we obtained only a few and very small crystals. As already shown for the PC rod structure [16], there is stronger electron density in the center rod cavity (as compared with the electron density from PC trimer crystal structures) contributed by the presence of the many different linker proteins, superimposed one on the other (Fig. 4). We could not identify significant density for GA molecules in the structure most likely due to the randomness of GA cross-linking.

3.5. Electron microscope analysis of TvPBS and AmPBS

The major source of structural information on the entire PBS has been previously obtained from TEM analysis of negatively stained PBS isolated in HPB. When freshly prepared Tv-hpPBS, isolated from a sucrose gradient at 1.5 M sucrose and 0.9 M phosphate were visualized by TEM using typical negative-staining protocols, we found that stain did not penetrate the particles efficiently and the resulting complexes are not well-resolved. We found however that when the sample was pre-incubated at 60 °C (the optimal growth temperature of *T. vulcanus*) for 2 min, before application onto the EM grid, stain was able to penetrate more efficiently, and single complexes could be identified (Fig. 5A). The precise affect of the temperature treatment on the complexes is not clear; however it may be that in the case of Tv-PBS remnants of the sucrose gradient both sucrose and/or HPB prevent proper staining and the elevated temperature promotes their removal. In these complexes, it appeared that TvPBS indeed has a pentacylindrical core (Fig. 5A, insert) and not a tricylindrical core as has been proposed for the highly homologous *T. elongatus* [23]. While only four rods surround the core, the core itself appears to be intact and to contain five elements, alluding to its pentacylindrical nature. It should be noted that most particles did not appear to have a regular structure, indicating either extreme instability of the complex, or that the organization of the TvPBS is not as ordered as proposed for other PBSs. Our conclusion that TvPBS is pentacylindrical is supported not only by the presence of the entire 127 kDa ApcE linker in the Tv-hpPBS crystals (Table 1), but also by measurement of the PC/APC ratio which was found to be 1.5 ± 0.2, which correlates to a PBS composed of 24 PC trimers and 16 APC trimers. This ratio is indicative of a PBS that has a pentacylindrical core surrounded by six rods of 2 hexamers in each rod.

Negative-stained TEM was also performed on Tv-clPBS. In this case the temperature pre-treatment was not required. The micrographs visualize compact globular particles with diameter of 29.5 ± 3.3 nm (Fig. 5B). The complexes are very reminiscent of the PBS of *Porphyridium cruentum* visualized by Boekema and co-workers [50]. In these complexes the rods appear to lay on the core and not to protrude out from the core as suggested in many of the PBS models. Negative stained TEM of Am-clPBS (Fig. 5C and D) presented rod-shaped complexes with dimensions of 23.5 ± 2.3 nm × 10 ± 1.4 nm confirming that cross-linking did not alter the rod-shaped architecture of the complex [44].

Since it appeared that the staining procedure did not result in easily interpretable EM data, we decided to attempt to visualize TvPBS frozen in vitreous ice (cryo-TEM). Since this necessitates removal of the high concentration of phosphate buffer (and thus has hampered previous attempts to perform cryo-TEM), we performed these measurements on the same Tv-clPBS samples used for crystallization. 3 μl of the sample was applied to the glow-discharged grid, blotted for 3–4 s and flash frozen in liquid ethane cooled by liquid nitrogen [45]. The images revealed large fields of relatively homogenous globular particles, with particle sizes estimated to be ~28 × 30 nm. Nearly 50,000 particles were selected and classified into 543 classes (Fig. 6A) followed by *ab initio* reconstruction of a preliminary model [46]. The final map was refined to 30 Å resolution, as determined by Fourier Shell Correlation (FSC) using the FSC = 0.143 criterion (Fig. 6B). The resulting electron density map (Fig. 6C, I–IV) shows an arrangement of 14 clearly defined densities, each with the dimensions of a PBP hexamer, interconnected by narrow bridges. One side of the map appears to form a dome-like structure (Fig. 6C, blue hexamers) and includes five hexamers. From this side, six elongated leg-like structures protrude, each with 1–2 hexamers (Fig. 6C, green hexamers). An additional body with the dimensions of a hexamer is found in the center of the particle (Fig. 6C, black hexamer). The resolution obtained does not afford clear identification of the hexamers as either PC or APC hexamers, as these objects have very nearly the same dimensions. It is appealing to assign the six "legs" to the six rods that emanate out from the core, with the remaining five hexamers belonging to the core. It is clear that the cross-linking procedure, while able to stabilize the structure and avoid disintegration, is not strong enough to hold the PBS in a structure that matches any of the proposed models. The molecular mass of 14 hexamers is 3.2 MDa which matches the calculated mass obtained by DLS, and the dimensions of the particle are about 31 × 28 × 28 nm, which is only slightly smaller than the measured hydrodynamic radius and similar to the negatively stained Tv-clPBS particles. Importantly, MS analysis shows the presence of all components, and the spectroscopic data clearly shows energy transfer from PC to APC, even though the complex has a completely different form than that proposed for classical PBS models.

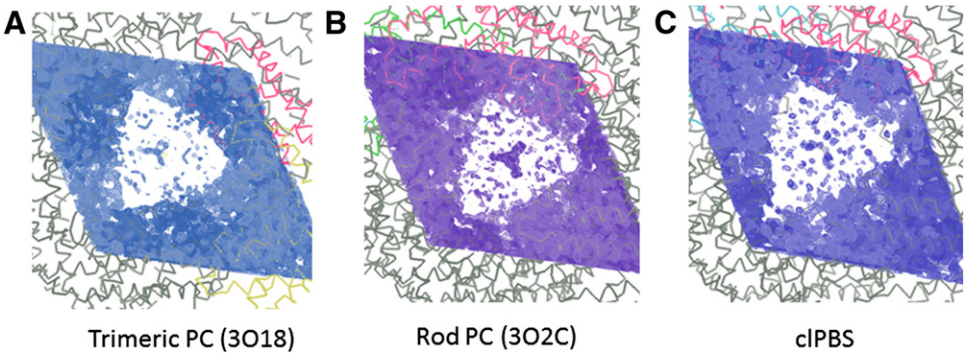

Fig. 4. 2Fo-Fc electron density maps centered on the hexameric aperture of different levels of assembly of PBS crystals. A) Trimeric PC (PDB ID: 3O18). B) Rod PC (PDB ID: 3O2C. C) Tv-clPBS (PDB ID: 4N6S). All structures have a monomer in the asymmetric unit and the trimer is formed by visualizing symmetry related molecules. All maps were calculated at 2.4 Å and are displayed at 2σ over the background density.

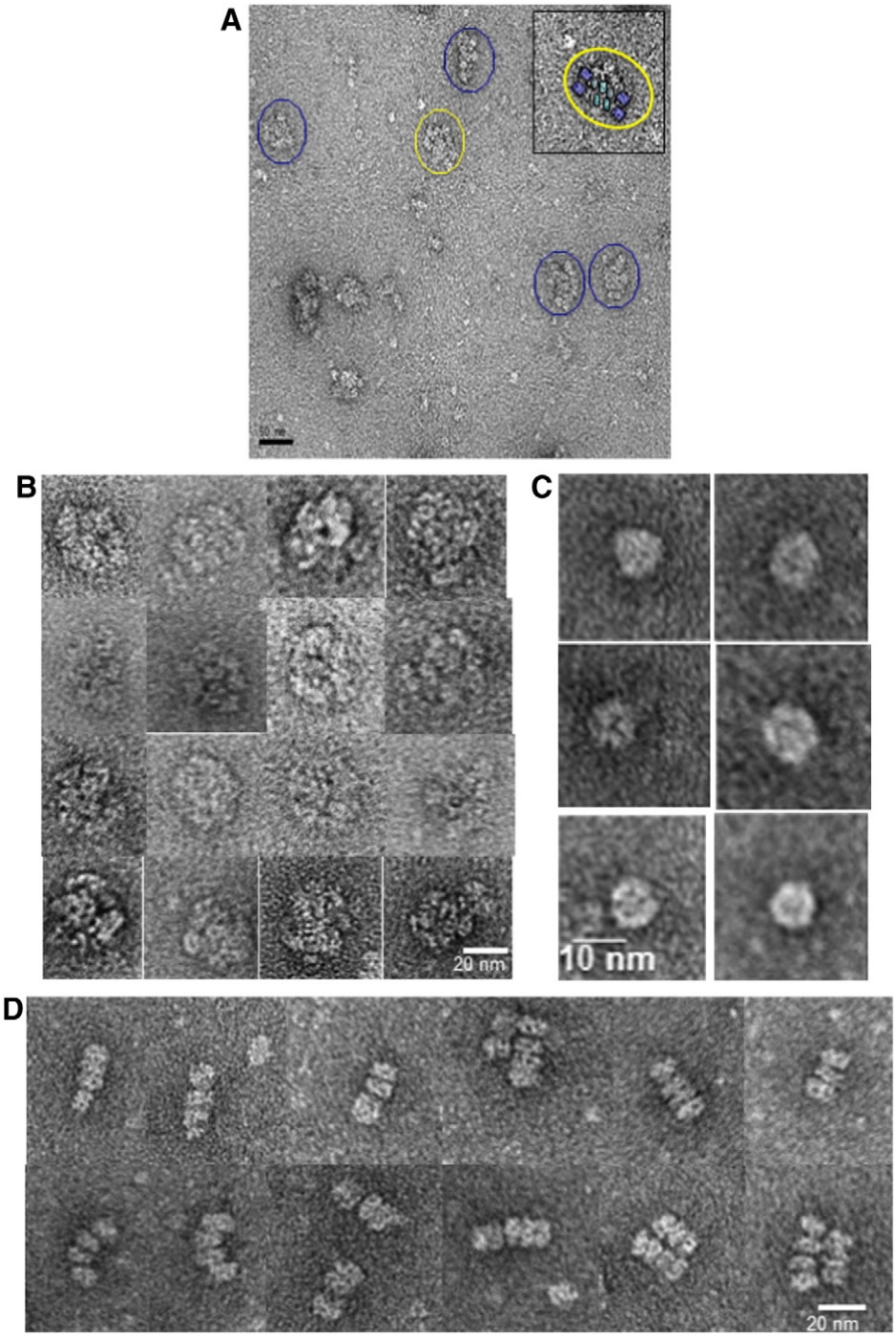

Fig. 5. Negatively-stained transmission electron microscope analysis of Tv-clPBS and Am-clPBS. (A) Negatively stained Tv-hpPBS obtained following a short incubation at 60 °C. Circles indicate different single complexes. Insert shown and enlargement of the particle encircled by the yellow circle in panel A. Cyan and blue graphic objects are overlaid onto the sites of five APC core cylinders and four PC rods, respectively. While only four rods are seen emanating from the core, the core itself appears intact. (B) Gallery of negatively-stained Tv-clPBS particles. (C) Gallery of negatively-stained Am-cl-PBS particles from the top (or bottom) dimension. (D) Gallery of negatively-stained Am-cl-PBS particles seen from the side. Following cross-linking and transfer to low ionic strength buffer, the isolated Tv-clPBS and Am-clPBS were washed again in 50 mM tris buffer prior to negative staining. Bars show image dimensions.

4. Discussion

Photosynthetic organisms have evolved a broad spectrum of solutions for efficient harvesting of light and transfer of this energy to the photochemical RCs [1]. In all systems, these different solutions embody similar functional characteristics, indicating their importance for the process. One such characteristic is the combination of outer LHCs, surrounding an interior LHC that is directly and stably coupled to the RC. Peripheral LHCs are typically a closed system (formed by symmetric oligomerization) that limits their total size, and thus their complement of chromophore molecules [2,5,14]. In most cases, the peripheral LHCs are composed of transmembrane proteins, thus limiting their ability to expand the number of directly associated LHCs with the RC. In order to increase the cross section of absorption for each RC (in order to drive photosynthesis under low light conditions), the two-dimensional limitation of the membrane dimension forces multiple copies of similar LHCs to assemble in the membrane plane, and absorbed energy will necessarily jump between complexes before reaching an RC. Absorbed energy must be transferred at high rates to avoid competing processes that might result in an overall decrease in

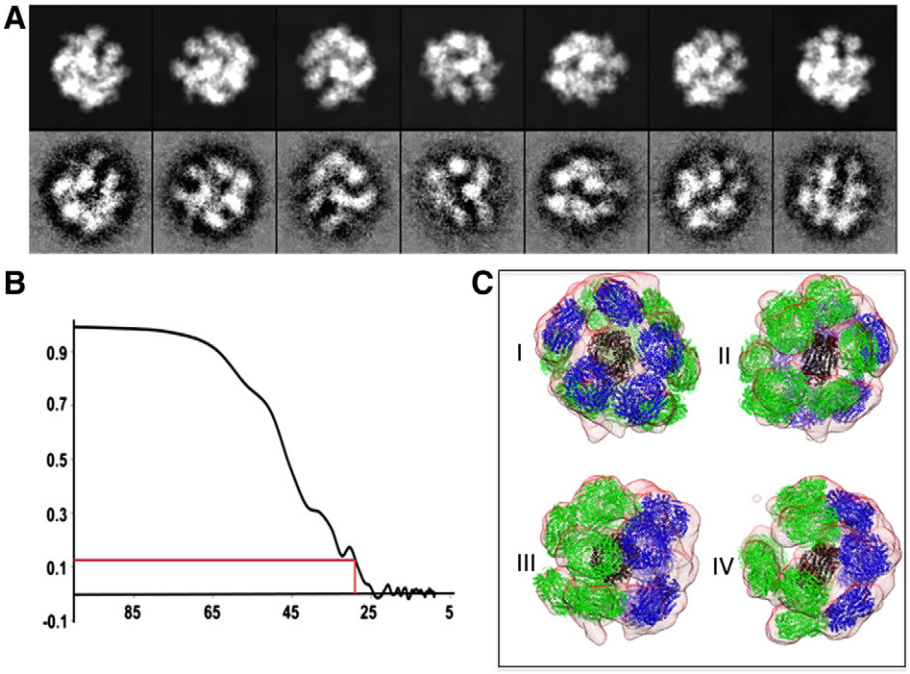

Fig. 6. Cryo-transmission electron microscopy analysis of Tv-clPBS. (A) Projections of the final reconstruction (top row) and class averages in corresponding orientations (bottom row) obtained from the 50,000 raw images. (B) Validation data for the single-particle three-dimensional reconstruction. Fourier shell correlation plot determines the resolution to ~30 Å according to the Fourier shell correlation = 0.143 criterion. (C) Refined cryo-TEM density map fitted with 14 phycobiliprotein hexamers. Docking into the EM map was performed using the chimera fit module. Five hexamers that appear to form a dome-like structure are in blue, eight hexamers that were docked into six elongated protrusions connected to the dome are in green, and a single hexamer docked into a central body is in black. (I), View of the particle from above the dome. (II), View from below the particle, looking onto the aperture formed by the six appendages. (III) and (IV), Two side views of the particle.

photosynthetic efficiency. Coupled with the architectural factors mentioned above, the relative orientations of all of the chromophores within the peripheral LHCs, as well as the orientations between chromophores in adjacent complexes are quite constant (for each system) and not just a random aggregation of pigments. It is most likely that the chromophore orientations have been evolutionarily optimized for energy transfer within each LHC, between peripheral LHCs and from peripheral LHCs to the internal, stable LHC/RC photosystems.

In the PBS, the complex is assembled from two large substructures, the rods and core. The core itself is an assembly of cylinders with dimensions similar to those of rods. Crystal structures of the isolated components (PE, PC and APC), show that potential steps in assembly from trimer to hexamer (and perhaps further) are similar. The major mode of assembly orients all of the bilin chromophores in orderly, identical orientations. As described above, we typically assume that an assembly of this fashion is optimal for energy transfer along the rods or within the core cylinders. Another important aspect of PBS assembly is that rods and core cylinders all have three-fold symmetry, which may be very slightly broken by the asymmetry in the associated LPs running through the rod and core cavities.

The PBS of *A. marina* takes this element of assembly one step further, placing its single APC trimer within the single rod structure. In this fashion, the six APC chromophores occupy the same spatial positions of six of the nine PC chromophores of the adjacent trimer, similar to all of the internal (α84 and β84) chromophores along the rod. Indeed, energy transfer to APC in AmPBS is quite efficient [39].

Aside from the AmPBS, all other PBS complexes have been described as having the rods protruding out from the core. Indeed, many published TEM images show this arrangement, although none are as clearly structurally homogeneous as LHI and LHII from purple bacteria, or LHCII from plants or green algae. Indeed, many published EM studies show many complexes that are far from complete, showing the rods in many different angles protruding out from the core. This lack of homogeneity has been attributed to the known lack of PBS complex stability, and the requirement of HPB to preserve some semblance of order. The PBS has been successfully reconstituted from isolated subfractions from different organisms [47–49], on the basis of energy transfer. TEM analysis of the reconstituted complexes indeed showed the formation of complexes; however the level of order in the assembly is lower than in the original complex. These results agree with our suggestion that the rods do not in fact need to be in a single, highly ordered position with respect to the core in order to transfer energy at an efficiency greater than 90% [7,8]. A very recent study has described the existence of PBS:PSII:PSI megacomplexes in *Synechocystis* sp. PCC 6803. In this arrangement, the same architecture of the PBS is proposed to be able to provide energy transfer to both PSII (*via* ApcE in the core) and PSI (*via* ApcD in the core), although the geometry of association is quite different [50].

In any case, the arrangement of the rods in the popular fanned out fashion from the core brings the rods into a diametrically different geometric relationship with the core cylinders (Fig. S1, A and B). This change in alignment will also change the relative orientation of the chromophores (Fig. S2, I and II). If the chromophores in the rods and cylinders are optimized for directed energy transfer, why would this "kink" in the energy transfer pathway exist? One possibility is that this radical change in geometry brings the rod's terminal chromophores into closer proximity to the cylinder chromophores. A second possibility is that the change in geometry introduces a change in the kinetics of energy transfer from rods to core, required for proper kinetic matching between the tremendous light harvesting capabilities of the enormous PBS, with the functional capabilities of the RC (especially that of PSII) that lie beneath it. A third possibility is that the accepted model of rods surrounding the core is incorrect (or only partially correct) and what has been visualized by TEM represents only a sub-fraction of the isolated complexes. There is a possibility that the rods loosely associate with the core at different angles — some rod-edge to core cylinder (as in the most prevalent model), some rod-edge to core edge (Figs. S1, C and S2, II — an arrangement closer to the *A. marina* geometry) and still others where the rods associate along the core cylinders, providing contact between the rods' outer β155 chromophores and the core

(Figs. S1, D and S2, III). While certainly less visually appealing, this arrangement does not require tight binding to specific sites; rather, this arrangement implies that as long as there are rod chromophores positioned within 2–3 nm of the core chromophores, energy transfer will be as efficient as required by the entire photosynthetic system. This arrangement might explain why the rods so easily lose their interaction with the core when removed from the crowded cytoplasmic environment in the absence of HPB. Single particle analysis of negatively stained PBS from *Porphyridium cruentum* [51] indeed appear to show rods lying on the core, and not jutting out. An AFM study of *P. cruentum* PBS complexes, probed *in situ* on the thylakoid membrane [52], is one of the highest resolution visualizations of the PBS in its native environment. These measurements do not portray a complex that is similar to those seen in negatively stained TEM images. The PBSs are very crowded, and rods are also packed together over the cores. The tight packing of PBS on the membranes has been shown elsewhere, and may strengthen the hypothesis that rods do not associate with the cores in a fashion seen by negative staining. On the other hand, some measurements indicate that the PBS is quite mobile [53–55]. This has been interpreted as an indication of loose packing of PBS, which is contradiction with the AFM and TEM studies. In the least, these contradictions show that projecting the structure of the PBS only on the basis of isolated complexes may be problematic.

In this study, we used a variety of methods to obtain high-resolution structural details on the entire PBS, especially the mode of rod association to the core. Chemical crosslinking provided stable complexes in the absence of HPB that continue to exhibit almost total energy transfer from PC to APC. The cross-linking was designed to be minimal, to ensure that each complex is stabilized while limiting intercomplex linking. On the basis of the crystal structure presented here, the crosslinking was strong enough to prevent complex disintegration, but not strong enough to prevent movement of hexamers, and thus the crystallization forces pushed the units into the most stable lattice, that of elongated rods. While obviously completely different than the accepted PBS fan-like structure, energy transfer within the crystal is efficient. The single particle analysis of the cryo-TEM images of the Tv-clPBS shows particles in which rod like appendages are connected to a central body composed of hexameric objects. We could not, at the resolution obtained, determine the positions of the PC or APC containing hexamers, nor could we identify the linkers (especially ApcE). However, these particles, stable in low ionic strength buffer, efficiently transfer energy from PC to APC. Taken together we show here that at least for the TvPBS and AmPBS, rod PC efficiently transfers energy to core APC, regardless of mode of association.

The results presented here further illuminate the need to study the PBS, both structurally and functionally in its native environment, associated with the thylakoid membrane[56,57]. In many cases this has been hampered by the fact that PBS complexes are packed so closely to one another that it is difficult to ascertain the boundaries that delineate each complex. This very packed environment may hold within it the reason behind the intrinsic instability of the isolated PBS, and agrees with the model proposed here that permits different angles of association of the rods onto the cores without loss of energy transfer functionalities.

Supplementary data to this article can be found online at http://dx.doi.org/10.1016/j.bbabio.2013.12.014.

Acknowledgements

This work was supported by the US–Israel Bi-National Science Foundation (2009406) and the Israel Science Foundation founded by the Israel Academy of Sciences and Humanities (1576/12). We also acknowledge the support from the Nancy and Stephen Grand Technion Energy Program (GTEP) and The Technion Russell Berrie Nanotechnology Institute (RBNI). We gratefully thank the staff of the European Synchrotron Radiation Facility (beamlines ID-23-1, ID23-2) for provision of synchrotron radiation facilities and assistance. We thank Diana Kirilovsky for providing facilities for TEM. We also thank David Bushnell for his technical assistance in the collection of the cryo-TEM images. LD was the recipient of a scientific exchange grant from the Photosynthetic Antenna Research Center, an Energy Frontier Research Center funded by the U.S. Department of Energy (DOE), Office of Basic Energy Science (grant no. DE-SC 0001035 to R.E.B).

References

[1] R.J. Cogdell, A.T. Gardiner, H. Hashimoto, T.H. Brotosudarmo, A comparative look at the first few milliseconds of the light reactions of photosynthesis, Photochem. Photobiol. Sci. 7 (2008) 1150–1158.
[2] Y.C. Cheng, G.R. Fleming, Dynamics of light harvesting in photosynthesis, Annu. Rev. Phys. Chem. 60 (2009) 241–262.
[3] N. Adir, Structure of the phycobilisome antennae in cyanobacteria and red algae, in: P. Fromme (Ed.), Photosynthetic Protein Complexes: A Structural Approach, WILEY-VCH Verlag GmbH & Co. KGaA, Weinheim, 2008, pp. 243–274.
[4] L.K. Anderson, C.M. Toole, A model for early events in the assembly pathway of cyanobacterial phycobilisomes, Mol. Microbiol. 30 (1998) 467–474.
[5] R.J. Cogdell, A.T. Gardiner, A.W. Roszak, C.J. Law, J. Southall, N.W. Isaacs, Rings, ellipses and horseshoes: how purple bacteria harvest solar energy, Photosynth. Res. 81 (2004) 207–214.
[6] A.R. Grossman, M.R. Schaefer, G.G. Chiang, J.L. Collier, The phycobilisome, a light-harvesting complex responsive to environmental conditions, Microbiol. Rev. 57 (1993) 725–749.
[7] A.N. Glazer, Light guides. Directional energy transfer in a photosynthetic antenna, J. Biol. Chem. 264 (1989) 1–4.
[8] R. MacColl, Cyanobacterial phycobilisomes, J. Struct. Biol. 124 (1998) 311–334.
[9] N. Adir, Elucidation of the molecular structures of components of the phycobilisome: reconstructing a giant, Photosynth. Res. 85 (2005) 15–32.
[10] N. Adir, M. Dines, M. Klartag, A. McGregor, M. Melamed-Frank, Assembly and disassembly of phycobilisomes, in: J.M. Shively (Ed.), Microbiology Monographs: Inclusions in Prokaryotes, vol. 2, Springer, Berlin/Heidelberg, 2006, pp. 47–77.
[11] W. Reuter, G. Wiegand, R. Huber, M.E. Than, Structural analysis at 2.2 A of orthorhombic crystals presents the asymmetry of the allophycocyanin-linker complex, AP.LC7.8, from phycobilisomes of *Mastigocladus laminosus*, Proc. Natl. Acad. Sci. U. S. A. 96 (1999) 1363–1368.
[12] R.J. Cogdell, A. Gall, J. Kohler, The architecture and function of the light-harvesting apparatus of purple bacteria: from single molecules to *in vivo* membranes, Q. Rev. Biophys. 39 (2006) 227–324.
[13] T. Barros, A. Royant, J. Standfuss, A. Dreuw, W. Kuhlbrandt, Crystal structure of plant light-harvesting complex shows the active, energy-transmitting state, EMBO J. 28 (2009) 298–306.
[14] Z. Liu, H. Yan, K. Wang, T. Kuang, J. Zhang, L. Gui, X. An, W. Chang, Crystal structure of spinach major light-harvesting complex at 2.72 A resolution, Nature 428 (2004) 287–292.
[15] A. Amunts, H. Toporik, A. Borovikova, N. Nelson, Structure determination and improved model of plant photosystem I, J. Biol. Chem. 285 (2010) 3478–3486.
[16] L. David, A. Marx, N. Adir, High-resolution crystal structures of trimeric and rod phycocyanin, J. Mol. Biol. 405 (2011) 201–213.
[17] E. Gantt, S.F. Conti, Granules associated with the chloroplast lamellae of *Porphyridium cruentum*, J. Cell Biol. 29 (1966) 423–434.
[18] E. Gantt, S.F. Conti, Phycobiliprotein localization in algae, Brookhaven Symp. Biol. 19 (1966) 393–405.
[19] E. Gantt, C.A. Lipschultz, Phycobilisomes of *Porphyridium cruentum*. I. Isolation, J. Cell Biol. 54 (1972) 313–324.
[20] G. Yamanaka, A.N. Glazer, R.C. Williams, Cyanobacterial phycobilisomes. Characterization of the phycobilisomes of *Synechococcus* sp. 6301, J. Biol. Chem. 253 (1978) 8303–8310.
[21] G. Yamanaka, D.J. Lundell, A.N. Glazer, Molecular architecture of a light-harvesting antenna. Isolation and characterization of phycobilisome subassembly particles, J. Biol. Chem. 257 (1982) 4077–4086.
[22] A.A. Arteni, G. Ajlani, E.J. Boekema, Structural organisation of phycobilisomes from *Synechocystis* sp. strain PCC6803 and their interaction with the membrane, Biochim. Biophys. Acta 1787 (2009) 272–279.
[23] J. Barber, E.P. Morris, P.C. da Fonseca, Interaction of the allophycocyanin core complex with photosystem II, Photochem. Photobiol. Sci. 2 (2003) 536–541.
[24] M. Watanabe, M. Ikeuchi, Phycobilisome: architecture of a light-harvesting supercomplex, Photosynth. Res. 116 (2–3) (2013) 265–276.
[25] A.G.W. Leslie, Recent changes to the MOSFLM package for processing film and image plate data Joint CCP4 + ESF-EAMCB Newsletter on Protein Crystallography, No. 26, 1992.
[26] A.J. McCoy, R.W. Grosse-Kunstleve, P.D. Adams, M.D. Winn, L.C. Storoni, R.J. Read, Phaser crystallographic software, J. Appl. Crystallogr. 40 (2007) 658–674.
[27] A.T. Brunger, P.D. Adams, G.M. Clore, W.L. DeLano, P. Gros, R.W. Grosse-Kunstleve, J.S. Jiang, J. Kuszewski, M. Nilges, N.S. Pannu, R.J. Read, L.M. Rice, T. Simonson, G.L. Warren, Crystallography & NMR system: a new software suite for macromolecular structure determination, Acta Crystallogr. D Biol. Crystallogr. 54 (1998) 905–921.
[28] P. Emsley, K. Cowtan, Coot: model-building tools for molecular graphics, Acta Crystallogr. D Biol. Crystallogr. 60 (2004) 2126–2132.
[29] W.L. DeLano, The PyMOL Molecular Graphics System, http://www.pymol.org 2002.
[30] J. Frank, M. Radermacher, P. Penczek, J. Zhu, Y. Li, M. Ladjadj, A. Leith, SPIDER and WEB: processing and visualization of images in 3D electron microscopy and related fields, J. Struct. Biol. 116 (1996) 190–199.

[31] S.J. Ludtke, P.R. Baldwin, W. Chiu, EMAN: semiautomated software for high-resolution single-particle reconstructions, J. Struct. Biol. 128 (1999) 82–97.
[32] D. Elmlund, H. Elmlund, SIMPLE: software for ab initio reconstruction of heterogeneous single-particles, J. Struct. Biol. 180 (2012) 420–427.
[33] B. Kastner, N. Fischer, M.M. Golas, B. Sander, P. Dube, D. Boehringer, K. Hartmuth, J. Deckert, F. Hauer, E. Wolf, H. Uchtenhagen, H. Urlaub, F. Herzog, J.M. Peters, D. Poerschke, x00Fc, R. hrmann, H. Stark, GraFix: sample preparation for single-particle electron cryomicroscopy, Nat. Methods 5 (2008) 53–55.
[34] L. David, N. Adir, Isolation of intact phycobilisomes in low salt: a novel method for purifying phycobilisomes by mild cross-linking, Photosynthesis Research for Food, Fuel and the Future, Springer, Berlin Heidelberg, 2013, pp. 143–147.
[35] H. Schiller, H. Senger, H. Miyashita, S. Miyachi, H. Dau, Light-harvesting in *Acaryochloris marina* — spectroscopic characterization of a chlorophyll d-dominated photosynthetic antenna system, FEBS Lett. 410 (1997) 433–436.
[36] M. Chen, T.S. Bibby, J. Nield, A.W.D. Larkum, J. Barber, Structure of a large photosystem II supercomplex from *Acaryochloris marina*, FEBS Lett. 579 (2005) 1306–1310.
[37] M. Chen, M. Floetenmeyer, T.S. Bibby, Supramolecular organization of phycobiliproteins in the chlorophyll d-containing cyanobacterium *Acaryochloris marina*, FEBS Lett. 583 (2009) 2535–2539.
[38] Q. Hu, J. Marquardt, I. Iwasaki, H. Miyashita, N. Kurano, E. Morschel, S. Miyachi, Molecular structure, localization and function of biliproteins in the chlorophyll a/d containing oxygenic photosynthetic prokaryote *Acaryochloris marina*, Biochim. Biophys. Acta Bioenerg. 1412 (1999) 250–261.
[39] C. Theiss, F.J. Schmitt, J. Pieper, C. Nganou, M. Grehn, M. Vitali, R. Olliges, H.J. Eichler, H.J. Eckert, Excitation energy transfer in intact cells and in the phycobiliprotein antennae of the chlorophyll d containing cyanobacterium *Acaryochloris marina*, J. Plant Physiol. 168 (2011) 1473–1487.
[40] E.L. Elson, Fluorescence correlation spectroscopy: past, present, future, Biophys. J. 101 (2011) 2855–2870.
[41] B.A. Zilinskas, R.E. Glick, Noncovalent intermolecular forces in phycobilisomes of *Porphyridium cruentum*, Plant Physiol. 68 (1981) 447–452.
[42] L. David, Structure determination of the phycobilisome complex, Chemistry, vol. Ph.D, Technion, Haifa, 2012, p. 110.
[43] CCP4, The CCP4 suite: programs for protein crystallography, Acta Cryst. D50 (1994) 760–763.
[44] J. Marquardt, H. Senger, H. Miyashita, S. Miyachi, E. Moerschel, Isolation and characterization of biliprotein aggregates from *Acaryochloris marina*, a Prochloron-like prokaryote containing mainly chlorophyll d, FEBS Lett. 410 (1997) 428–432.
[45] J. Lepault, F.P. Booy, J. Dubochet, Electron microscopy of frozen biological suspensions, J. Microsc. 129 (1983) 89–102.
[46] D. Elmlund, R. Davis, H. Elmlund, Ab initio structure determination from electron microscopic images of single molecules coexisting in different functional states, Structure 18 (2010) 777–786.
[47] O. Canaani, E. Gantt, Formation of hybrid phycobilisomes by association of phycobiliproteins from *Nostoc* and *Fremyella*, Proc. Natl. Acad. Sci. U. S. A. 79 (1982) 5277–5281.
[48] O. Canaani, C.A. Lipschultz, E. Gantt, Reassembly of phycobilisomes from allophycocyanin and a phycocyanin–phycoerythrin complex, FEBS Lett. 115 (1980) 225–229.
[49] R.E. Glick, B.A. Zilinskas, Role of the colorless polypeptides in phycobilisome reconstitution from separated phycobiliproteins, Plant Physiol. 69 (1982) 991–997.
[50] H. Liu, H. Zhang, D.M. Niedzwiedzki, M. Prado, G. He, M.L. Gross, R.E. Blankenship, Phycobilisomes supply excitations to both photosystems in a megacomplex in cyanobacteria, Science 342 (2013) 1104–1107.
[51] A.A. Arteni, L.N. Liu, T.J. Aartsma, Y.Z. Zhang, B.C. Zhou, E.J. Boekema, Structure and organization of phycobilisomes on membranes of the red alga *Porphyridium cruentum*, Photosynth. Res. 95 (2008) 169–174.
[52] L.N. Liu, T.J. Aartsma, J.C. Thomas, G.E. Lamers, B.C. Zhou, Y.Z. Zhang, Watching the native supramolecular architecture of photosynthetic membrane in red algae: topography of phycobilisomes and their crowding, diverse distribution patterns, J. Biol. Chem. 283 (2008) 34946–34953.
[53] C.W. Mullineaux, M.J. Tobin, G.R. Jones, Mobility of photosynthetic complexes in thylakoid membranes, Nature 390 (1997) 421–424.
[54] R. Kana, Mobility of photosynthetic proteins, Photosynth. Res. 116 (2–3) (2013) 465–479.
[55] C.W. Mullineaux, Phycobilisome-reaction centre interaction in cyanobacteria, Photosynth. Res. 95 (2008) 175–182.
[56] E. Tamary, V. Kiss, R. Nevo, Z. Adam, G. Bernat, S. Rexroth, M. Rogner, Z. Reich, Structural and functional alterations of cyanobacterial phycobilisomes induced by high-light stress, Biochim. Biophys. Acta 1817 (2012) 319–327.
[57] S.B. Krumova, S.P. Laptenok, J.W. Borst, B. Ughy, Z. Gombos, G. Ajlani, H. van Amerongen, Monitoring photosynthesis in individual cells of *Synechocystis* sp. PCC 6803 on a picosecond timescale, Biophys. J. 99 (2010) 2006–2015.